

Near-Source Ground Motion from Steady State Dynamic Rupture Pulses

Eric M. Dunham

Department of Physics, University of California, Santa Barbara, California, USA

Ralph J. Archuleta

Institute for Crustal Studies and Department of Geological Sciences, University of California, Santa Barbara, California, USA

Submitted to *Geophysical Research Letters* on 19 October 2004

Ground motion from two-dimensional steady state dynamic ruptures is examined for both subshear and supershear rupture velocities. Synthetic seismograms demonstrate that coherent high-frequency information about the source process rapidly attenuates with distance from the fault for subshear ruptures. Such records provide almost no resolution of the spatial extent of the stress breakdown zone. At supershear speeds, S waves radiate away from the fault, preserving the full source spectrum and carrying an exact history of the slip velocity on both the fault-parallel and fault-normal components of motion, whose amplitudes are given by a function of rupture speed that vanishes at $\sqrt{2}$ times the S wave speed. The energy liberated from the strain field by the passage of a supershear rupture is partitioned into fracture energy dissipated within the fault zone and far-field S wave radiation. The partition depends on both the rupture velocity and the size of the breakdown zone.

1. Introduction

Evidence for ruptures exceeding the S wave speed continues to mount, most recently in the 2002 M_w 7.9 Denali Fault, Alaska, earthquake [Ellsworth *et al.*, 2004; Dunham and Archuleta, 2005]. The ground motion recorded 3 km from the fault at Pump Station 10 along the Trans Alaska Pipeline System exhibited a set of pulses unlike any previously recorded. In light of this record and to further explain features appearing in the model of this event by Dunham and Archuleta [2005], we turn our attention to the near-source ground motion of dynamic ruptures. In particular, we address the question of which dynamic rupture parameters are resolvable from near-source records, and how this depends on rupture speed.

As a starting model, we investigate two-dimensional (2D) rupture pulses of finite length L , propagating at some steady state velocity V in the positive x direction along the fault plane $y = 0$. We shall refer to the x and y directions as fault parallel (FP) and fault normal (FN). The material on either side of the fault is identical, isotropic, and linear elastic, with shear modulus μ and P and S wave speeds c_p and c_s . The steady state assumption implies that we are modeling only the coherent portion of fields due to a smooth rupture process, and not the incoherent high-frequency radiation that results from breaking through small-scale heterogeneities.

We specify the shear traction $\tau(x)$ within the slip zone (unlike kinematic models, which would specify slip), and set the slip velocity to zero outside the slip zone. Following Broberg [1978, 1989], expressions for the particle velocity and stress fields, both on and off of the fault, are written in terms of a single integral expression of $\tau(x)$ over the slip zone, weighted by a singular kernel. The expressions are derived in an electronic supplement¹. Rice *et al.* [2004] has recently evaluated the integral in closed form for the specific case of subshear ruptures in which the shear traction decreases linearly with distance behind the rupture front. In order to accommodate any general $\tau(x)$ and to extend the model to supershear speeds, we numerically evaluate this integral at each observation point, requiring quadrature routines specifically designed to handle integrable and Cauchy-type singularities in the integrand [Piessens *et al.*, 1983]. Furthermore, we may combine the velocity and stress fields to obtain the energy flux field, useful for visualizing the flow of energy in these steady state situations.

The elastic fields may be separated into dilatational and shear parts, each governed by the wave equation with the appropriate wave speed. Under steady state conditions, the governing equations become two-dimensional in $x - Vt$ and y . A general field f at speed V may be written as $f(t, x, y) = f^p(x - Vt, y) + f^s(x - Vt, y)$, where f^p and f^s result from a displacement field $\mathbf{u} = \mathbf{u}^p + \mathbf{u}^s$ satisfying $\nabla \times \mathbf{u}^p = 0$ and $\nabla \cdot \mathbf{u}^s = 0$. Using Fourier analysis, we write $f^j(x - Vt, y) = \int_{-\infty}^{\infty} \hat{f}^j(k_x) e^{ik_x(x-Vt)} e^{-k_x \alpha_j y} dk_x$, where $\alpha_j = \sqrt{1 - V^2/c_j^2}$ and $j = p$ or s . This simply decomposes the response into plane waves $e^{i(k_x x + k_y y - \omega t)}$, subject to the dispersion relation $\omega = c_j \sqrt{k_x^2 + k_y^2}$, and to the condition that the FP phase velocity equals the steady state velocity: $\omega/k_x = V$. For $V < c_s$, both the P and S waves are evanescent (i.e., inhomogeneous). The amplitude of the Fourier modes excited by the source process consequently decay exponentially with distance as the observation point moves away from the fault, with the decay length set by the magnitude of the FP wave number k_x and the velocity-dependent factor α_j . In contrast to this, when $c_s < V < c_p$, α_s becomes imaginary, and the S waves radiate away from the fault; i.e., $f^s(x - Vt, y) = \int_{-\infty}^{\infty} \hat{f}^s(k_x) e^{ik_x(x+\beta_s y - Vt)} dk_x$, where $\beta_s = \sqrt{V^2/c_s^2 - 1}$. The propagation angle of these waves with respect to the fault is simply the Mach angle.

Supporting material is available via Web browser or via Anonymous FTP from <ftp://ftp.agu.org/apend/> (Username = "anonymous", Password = "guest"). Subdirectories in the ftp site are arranged by journal and paper number. Information on searching and submitting electronic supplements is found at http://www.agu.org/pubs/esupp_about.html.

This implies that the shear field generated by the source process on the fault is transported without attenuation to observation points off of the fault. This remarkable property, not present for subshear ruptures, allows for a precise determination of the source properties from near-source records of supershear ruptures.

2. Subshear Ruptures

Let us begin with subshear ruptures. For simplicity, we take $t = 0$ such that $x - Vt \rightarrow x$ and place the origin of our coordinate system at the leading edge of the slip zone. We use the linear distance-weakening model of *Palmer and Rice* [1973] in which $\tau(x) = \tau_r + (\tau_p - \tau_r)x/R$ for $-R < x < 0$ and $\tau(x) = \tau_r$ for $-L < x < -R$. Figure 1 shows the velocity field at $V = 0.85c_s$ and $R/L = 0.25$ as well as synthetic seismograms at various distances away from the fault for several R/L . The motion is predominantly in the FN direction, and the synthetics are virtually identical to those from steady state kinematic models [e.g., *Luco and Anderson*, 1983]. As expected on the basis of the Fourier decomposition, increasing the distance between the observer and the fault filters the high frequency components of the wavefield excited by the source process [e.g., *Aki and Richards*, 2002, p.524]. Note that our results pertain only to the coherent portion of the spectrum resulting from a smooth rupture process. We can estimate the minimum resolvable wavelength for the shear component of the fields λ_{\min}^s at some distance y away from the fault in the following manner: Information at a particular frequency becomes irresolvable when its amplitude drops to some fraction, say 5%, of its amplitude on the fault, leading to the condition $e^{2\pi\alpha_s y / \lambda_{\min}^s} \sim 0.05$. For $V \sim 0.85c_s$, $\lambda_{\min}^s \sim y$, the distance between the station and the fault. An even stricter restriction exists for the dilatational fields. This can clearly be seen in Figure 1b when comparing the synthetic seismograms from the three ruptures, which have identical V , L , and total slip, but with R varying over an order of magnitude. This echoes a similar conclusion by *Guatteri and Spudich* [2000], and demonstrates the fundamental difficulty inversions face when using records from subshear ruptures, even without the finite bandwidth limitation from the instrumental response and scattering along the ray path. On the other hand, our analysis supports the use of kinematic modeling for sub-Rayleigh ruptures, and emphasizes that the parameterization of the slip velocity function will have little effect on the ground motion, so long as the final slip and rise time are preserved.

3. Supershear Ruptures

The ground motion from supershear ruptures has several remarkable properties, as revealed in Figure 2. Distinctive planar wavefronts emanate from the leading and trailing edges of the slip zone, as expected since the S waves radiate at these speeds. The angle that these wavefronts make with the fault is the Mach angle. Preceding the arrival of the Mach front is the dilatational field, characterized by a circular pattern of rotation around the slip zone. Unless the observer is on the fault, this results in predominantly FP motion, particularly as $V \rightarrow c_p$. In this limit, the P waves become homogeneous and propagate at grazing incidence to the fault with a purely FP particle motion.

The fields change character as V crosses $\sqrt{2}c_s$, the speed at which the S wave radiation vanishes [*Eshelby*, 1949]. This follows from the expression for the shear traction on the fault in terms of the displacement fields: $\sigma_{xy} = \mu(\partial u_x / \partial y + \partial u_y / \partial x)$, or in the plane wave basis: $\sigma_{xy} = \mu(ik_y u_x + ik_x u_y)$. Choosing a particular V sets both the

relative amplitudes of k_x and k_y and the ratio between u_x and u_y since it determines the propagation angle of the radiating wave with respect to the fault. At $V = \sqrt{2}c_s$, a precise balance occurs ($k_x = k_y$ and $u_x = -u_y$), from which it follows that such a wave exerts no shear force on the interface. Conversely, this implies that a change in shear traction on the fault (as we model the source process) does not excite S waves. As V crosses through $\sqrt{2}c_s$, the relative sign of stress and displacement reverses, resulting in a reversal of the S wave particle motion.

The ground motion from supershear ruptures contains a wealth of information. The shear field carries an exact history of the slip velocity on the fault that appears in both the FP and FN velocity components, as well as in all of the stress components. The velocity fields carried by the S waves are given by $v_x^s(x + \beta_s |y|) = 0.5 \text{sgn}(y)(\beta_s^2 - 1)/(\beta_s^2 + 1)\Delta v(x + \beta_s |y|)$ and $v_y(x + \beta_s |y|) = -(0.5/\beta_s)(\beta_s^2 - 1)/(\beta_s^2 + 1)\Delta v(x + \beta_s |y|)$, where $\Delta v(x)$ is the slip velocity on the fault. Consequently, the record from even a single station could be used to determine both V (from the FP to FN ratio) and Δv .

The direct transport of the slip velocity function off of the fault results in large amplitudes of both velocity and acceleration, particularly if R is small, as laboratory measurements seem to indicate. As discussed in the previous section, R cannot be reliably estimated from current (sub-Rayleigh) ground motion records. Consequently, the use of large values of R to resolve the breakdown process in numerical models will result in an underprediction of the peak ground velocity and acceleration when the rupture process is supershear.

Pump Station 10 from the Denali Fault earthquake offers the best near-source record of a supershear rupture; however, the station captured waveforms resulting from a particularly non-steady rupture process and exhibits motions characteristic of both supershear and subshear ruptures (Figure 3). In the dynamic model by *Dunham and Archuleta* [2005], the rupture accelerates from $0.6c_s$ to $1.5c_s$ approximately 25km before the station. This process generates a secondary slip pulse moving at the Rayleigh speed. Ground motion pulses A and B (which have a large FP to FN ratio) are generated by the supershear rupture, while pulses C and D (almost entirely on the FN component) arise from the secondary subshear slip pulse. The rapid downward swing in pulse B marks the arrival of the shear field (compare with Figure 2d). Direct extraction of the slip velocity function from the record is not possible for two reasons. The transient emergence of the supershear rupture just prior to the station causes nearly simultaneous arrival of the dilatational and shear field. Furthermore, motions from the secondary slip pulse appear in the tail of the supershear motions. The two-sided FN motions (C and D) are exactly those expected from a subshear slip pulse (compare with Figure 1b), with C being associated with the leading edge of the slip zone and D with the trailing edge. This constrains the width of the slip pulse to approximately 15 km, much larger than appears in the model by *Dunham and Archuleta* [2005], who chose parameters to match the narrowness of pulses A and B (at the expense of truncating the width of the secondary slip pulse). The record leaves an open question: What type of rupture process or friction law results in a remarkably narrow supershear rupture pulse but quite broad subshear slip pulse?

4. Energy Balance

The energy balance for dynamic ruptures changes considerably at supershear speeds. For subshear speeds, steady

state pulses excite only evanescent waves that do not radiate into the far field. Consequently, all of the strain energy liberated by allowing slip to temporarily relax the stress field dissipates within the fault zone as fracture energy [Rice *et al.*, 2004]. At supershear speeds, the S waves radiate and the flux of energy carried by these waves must be taken into account. The proper balance of energy (per unit area advance of the rupture) is $(\tau_0 - \tau_r)\delta = G + G_s$, where τ_0 is the initial (and final) shear traction far in front of (and behind) the slip zone, δ is the final slip, G is the fracture energy, and G_s is the radiated S wave energy (absent for $V < c_s$). The left member of this equation is the work done by the remote stress field in excess of the residual stress, which is the energy available for rupture from the elastic medium. The radiated S wave energy can be calculated by integrating the FN flux of energy over the slip zone: $G_s = 2g_s(V/c_s)\rho \int_{-L}^0 v_x^2(x, y = 0)dx$, where $g_s(V/c_s) = [(\beta_s^2 - 1)/(\beta_s^2 + 1)]^2/\beta_s$. Dimensional arguments require G (and G_s) to take the form $h(V/c_s, R/L)(\tau_p - \tau_r)^2 R/\mu$. For subshear ruptures h factors into two terms, the first dependent on V/c_s and the second on R/L . This factorization does not carry over to supershear ruptures [Broberg, 1989]. Figure 4 shows the partition of energy as a function of R/L and V/c_s . As R/L decreases, most of the energy is radiated, with the exception of a small range of velocities surrounding $\sqrt{2}c_s$, since no S waves are excited at this speed.

Acknowledgments. E.M.D. was supported by a National Defense Science and Engineering Graduate Research fellowship. This work was supported by a grant from the Keck Foundation which established an Interdisciplinary Program in Seismology and Materials Physics at UCSB. R.J.A. was partially supported by the Southern California Earthquake Center (SCEC). This is SCEC contribution number XXX. This is the Institute for Crustal Studies (ICS) contribution number XXX.

References

- Burridge, R., G. Conn, and L. B. Freund (1979), The stability of a rapid mode II shear crack with finite cohesive traction, *J. Geophys. Res.*, *85*, 2210–2222.
- Broberg, K. B. (1978), On transient sliding motion, *Geophys. J. Roy. Astr. Soc.*, *52*, 397–432.
- Broberg, K. B. (1989), The near-tip field at high crack velocities, *Int. J. Fract.*, *39*, 1–13.
- Dunham, E. M., and R. J. Archuleta (2005), Evidence for a supershear transient during the 2002 Denali Fault earthquake, *Bull. Seismol. Soc. Amer.*, in press.
- Ellsworth W. L., M. Celebi, J. R. Evans, E. G. Jensen, R. Kayen, M. C. Metz, D. J. Nyman, J. W. Roddick, P. Spudich, and C. D. Stephens (2004), Near-Field Ground Motions of the M 7.9 November 3, 2002, Denali Fault, Alaska, Earthquake Recorded at Pump Station 10, *Earthquake Spectra*, *20*, 597–615, doi:10.1193/1.1778172.
- Eshelby, J. D. (1949), Uniformly Moving Dislocations, *Proc. Roy. Soc. A*, *62*, 307–314.
- Gatteri, M., and P. Spudich (2000), What Can Strong-Motion Data Tell Us about Slip-Weakening Fault-Friction Laws, *Bull. Seismol. Soc. Amer.*, *90*, 98–116.
- Luco, J. E., and J. G. Anderson (1983), Steady state response of an elastic half-space to a moving dislocation of finite width, *Bull. Seismol. Soc. Amer.*, *73*, 1–22.
- Palmer, A. C., and J. R. Rice (1973), The Growth of Slip Surfaces in the Progressive Failure of Overconsolidated Clay, *Proc. Roy. Soc. London A*, *332*, 527–548.
- Piessens, R., E. de Doncker-Kapenger, C. W. Ueberhuber, and D. K. Kahaner (1983), *QUADPACK, A Subroutine Package for Automatic Integration*, Springer series in computational mathematics, vol. 1, 301 pp., Springer Verlag, New York.

Rice, J. R., C. G. Sammis, and R. Parsons (2004), Off-fault Secondary Failure Induced by a Dynamic Slip-Pulse, *Bull. Seismol. Soc. Amer.*, in press.

Eric M. Dunham, Department of Physics, University of California, Santa Barbara, CA 93106, USA. (edunham@physics.ucsb.edu)

Ralph J. Archuleta, Institute for Crustal Studies and Department of Geological Sciences, University of California, Santa Barbara, CA 93106, USA.

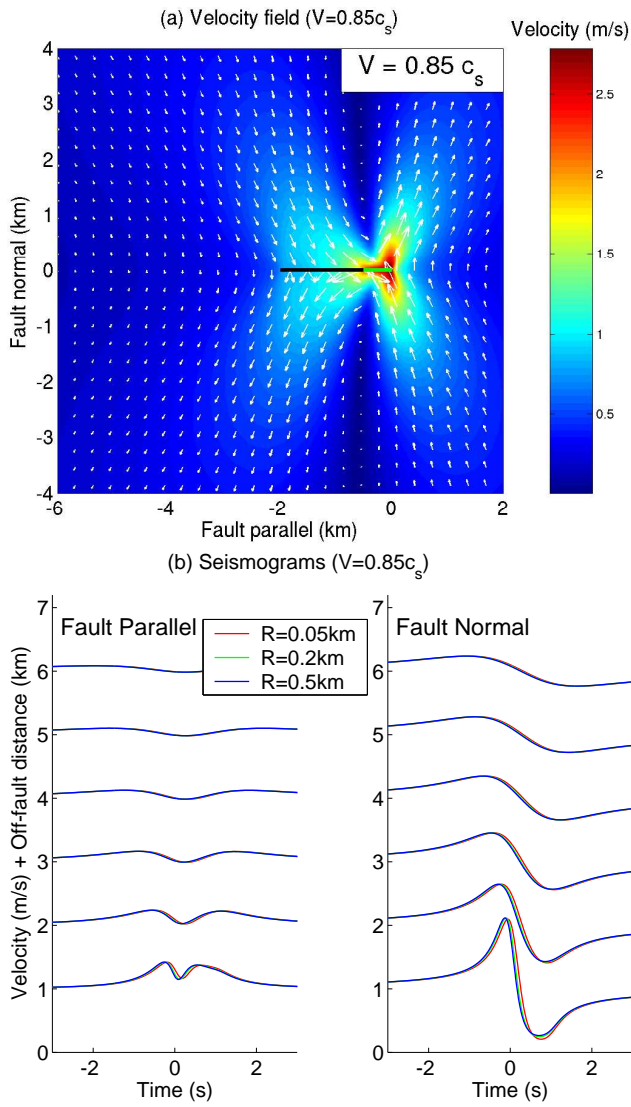


Figure 1. Velocity field (a) and synthetic seismograms (b) for a subshear rupture ($V = 0.85c_s$). In (a) the heavy black line denotes the slip zone and the heavy green line the breakdown zone. We take $\tau_p - \tau_r = 20\text{MPa}$, $\mu = 30\text{GPa}$, $L = 2\text{km}$, $c_p = 6\text{km/s}$, $c_p = \sqrt{3}c_s$, and $R = 0.5\text{km}$, unless otherwise noted. In (b) synthetic seismograms are computed for several values of R as labeled, holding the final slip fixed by varying $\tau_p - \tau_r$. For $R = 0.5$, 0.2 , and 0.05m , the equivalent slip-weakening distances (i.e., the slip at $x = -R$) are $D_c = 0.744$, 0.465 , and 0.231m , the strength drops are $\tau_p - \tau_r = 20.0$, 30.0 , and 58.71MPa , and the fracture energies are $G = 6.66$, 6.23 , and 6.03MJ/m^2 . Beyond several km from the fault, the records from all cases are indistinguishable.

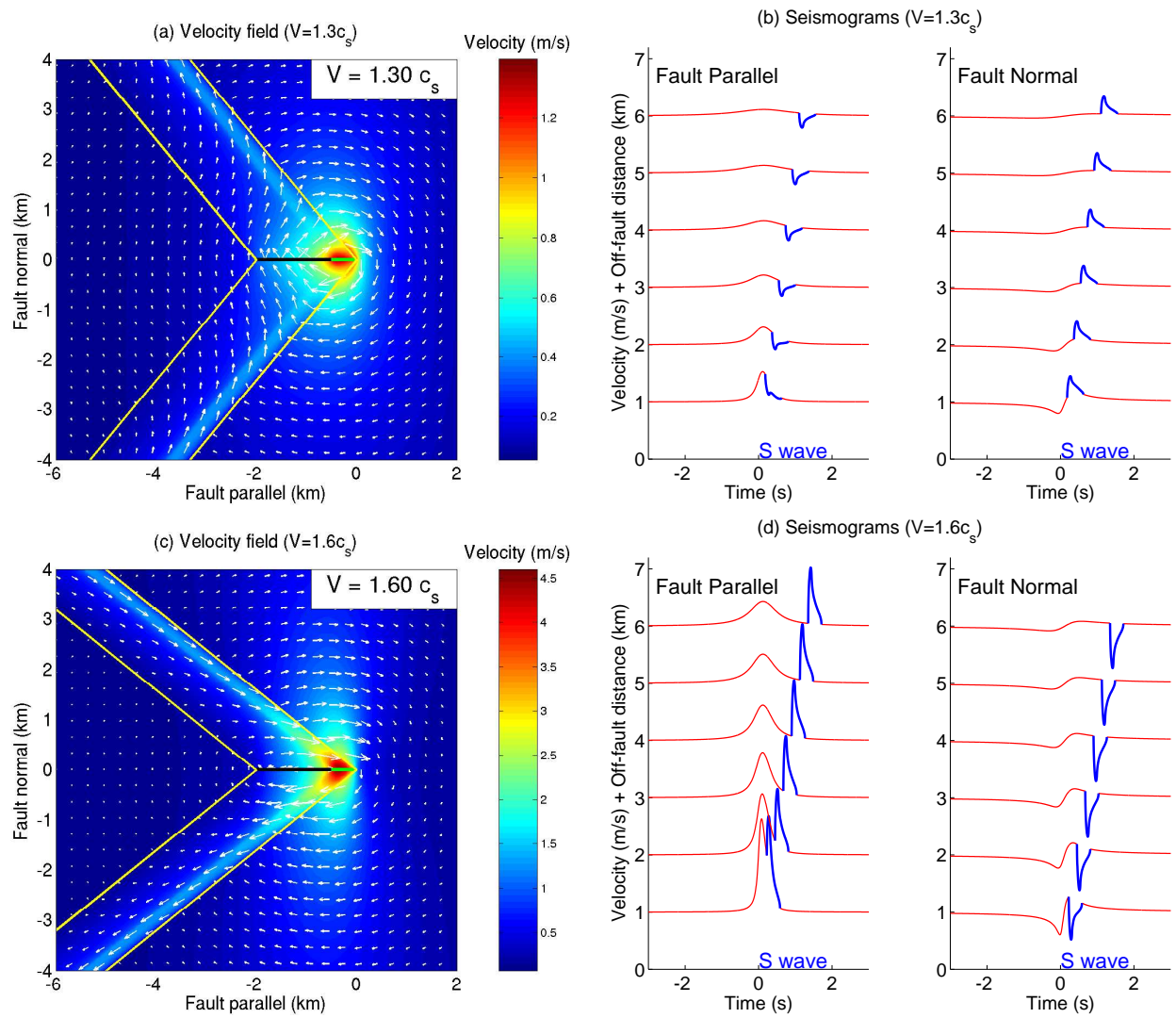


Figure 2. Velocity field (a and c) and synthetic seismograms (b and d) for supershear ruptures having speeds $V = 1.3c_s$ and $1.6c_s$. In (a) and (c) the heavy black line denotes the slip zone and the heavy green line the breakdown zone. The heavy blue lines in the seismograms mark the portions of the records during the passage of the radiated S waves. Parameters are given in the caption of Figure 1.

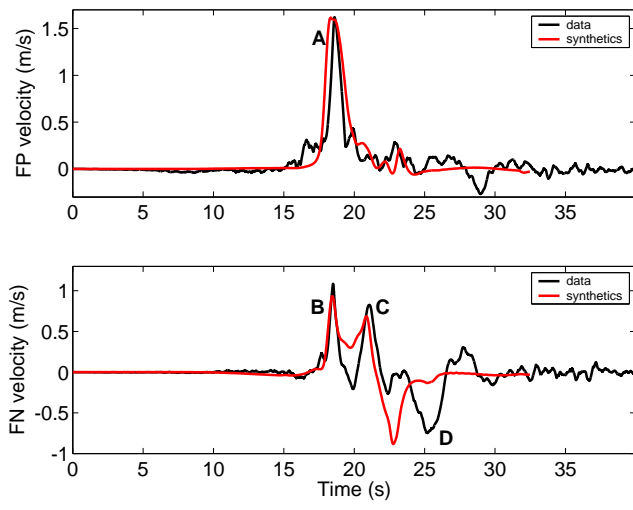


Figure 3. Data and synthetic seismograms for the Pump Station 10 record of the 2002 Denali Fault earthquake from the dynamic model by *Dunham and Archuleta*, [2005].

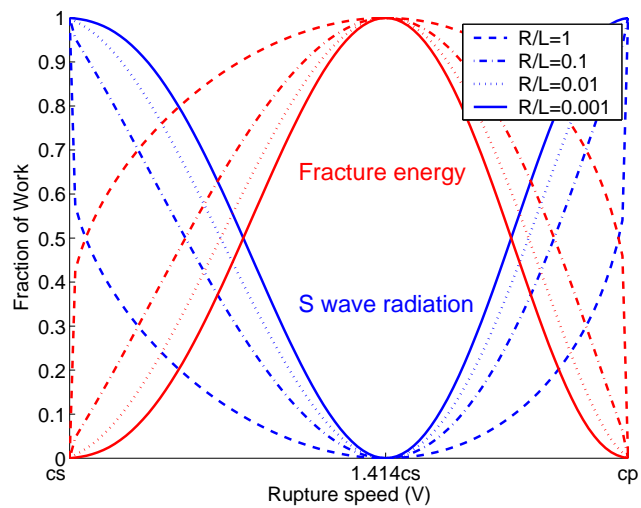


Figure 4. Energy partition between fracture energy and far-field S wave radiation for supershear ruptures as a function of V/c_s and R/L .